Supplementary Information - Mechanism of oxygen evolution and Mn_4CaO_5 cluster restoration in the natural water-oxidizing catalyst

Matteo Capone, Daniele Narzi* and Leonardo Guidoni*

Dipartimento di Scienze Fisiche e Chimiche, Universitá degli studi dellAquila, Via Vetoio (Coppito), 67100 LAquila, Italy

E-mail: daniele.narzi@univaq.it;leonardo.guidoni@univaq.it

Methods

All calculations here reported have been carried out using the CP2K package.[1] The classical portion of the protein was described by the AMBER99SB force field.[2] Other cofactors present in the PSII have been classically treated using the general AMBER force field (GAFF)[3] (see also Ref.[4,5]). The protonation state of the histidines bound to heme molecules, or directly interacting with iron atoms or the magnesium atom in chlorophylls was chosen in agreement with their relative orientation in the x-ray structure. The other titratable residues were considered in their standard protonation state. QM/MM calculations have been performed on a PSII model consisting of D1, D2 and CP43 protein domains, the respective cofactors and water molecules present in this region plus the Mn_4Ca cluster, starting from the x-ray structure resolved by Umena *et al* (PDB ID: 3ARC).[6] The Mn_4Ca cluster with its ligands present in the first shell (Asp170, Glu189, His332, Glu333, Asp342, Ala344, and CP43-

Glu354) plus additional residues in the second shell (Asp61, Tyr161, His190, His337, Ser169 and CP43-Arg357) have been treated at DFT level. Additionally, in the quantum region were included 4 water molecules directly coordinated with the Mn_4Ca cluster, the 10 closest water molecules and the chloride anion close to Glu333. The total charge of the quantum region and the MM region is 0 and -16 respectively.

The QM/MM MD simulations have been performed in NVT ensemble coupling the system with a thermal bath at room temperature 298.15 K using Nos-Hoover thermostat[7–9] (time constant $\tau_T = 0.1$ ps). Positions of the classical Cα atoms were kept fixed during the dynamic. A 28.0 Å side cubic cell and a cut-off for the plane-wave expansion of 320 Rydberg was used to treat the quantum region. The QM/MM model was centered in the cell in vacuum conditions. The PBE+U scheme[10–12] was employed with the `DZVP-MOLOPT-SR-GTH` Gaussian basis set optimized for molecular systems.[13] The electrostatic coupling between the the classical and the quantum region of the system was treated by means of fast Gaussian expansion of the electrostatic potential.[14] The systems have been simulated following the "high" oxidation state paradigm, consistently with previous works[15–18] A time step of 0.5 fs was used and the simulations have been carried out for 10 ps.

For minimum energy path calculations (MEP) the B3LYP functional have been used with the `TZVP-MOLOPT-SR-GTH` basis set. QM gas-phase models were extracted from the QM/MM simulations obtaining a homogeneous distribution on the selected reaction pathway through linear interpolation between the starting and the final geometries.

In order to obtain a reasonable state of the Mn_4Ca cluster with O_2 detached, necessary to subsequently built the reaction coordinate of the MEP calculation, we previously proceeded to perform a distance restrained QM/MM MD simulation, increasing smoothly Mn1-O6 and Mn3-O5 distances. We considered freshly formed O_2 as unbound from the Mn_4Ca cluster when the O_2 molecule do not fall backwards to bound state upon subsequent geometry optimization. Such meta-stable condition was reached for distances of Mn1-O6, Mn3-O6 and

Mn4-O6 equal to 2.49 Å,3.45 Å,3.38 Årespectively. In this condition, the O5-O6 distance decreases to 1.21 Å confirming the full formation of molecular oxygen with the typical double bond. The O6 atom results the closest oxygen to Mn3 while O5 is placed in a vertical position with respect to the Mn_4Ca cluster (see also Fig.2 in the main text).

MEP calculations describing the entrance of W3 into the cavity were preceded by a constrained QM/MM-MD simulation in which the Mn3-W3 and the intra-molecular O-H distances have been decreased up to the proton release from W3 to W2 and the relocation of W3 in the O5 position in the S_0 state. The final structure of the constrained QM/MM MD simulation was used as final point of the reaction coordinate in the MEP calculations.

MEP calculations describing the entrance of the hydroxide ion W2 were preceded by a constrained QM/MM-MD simulation in which the distance between W2 and Mn3 was decreased up to the bond formation between W2 and Mn3. The final structure of the simulation was used as final model of the respective reaction coordinate.

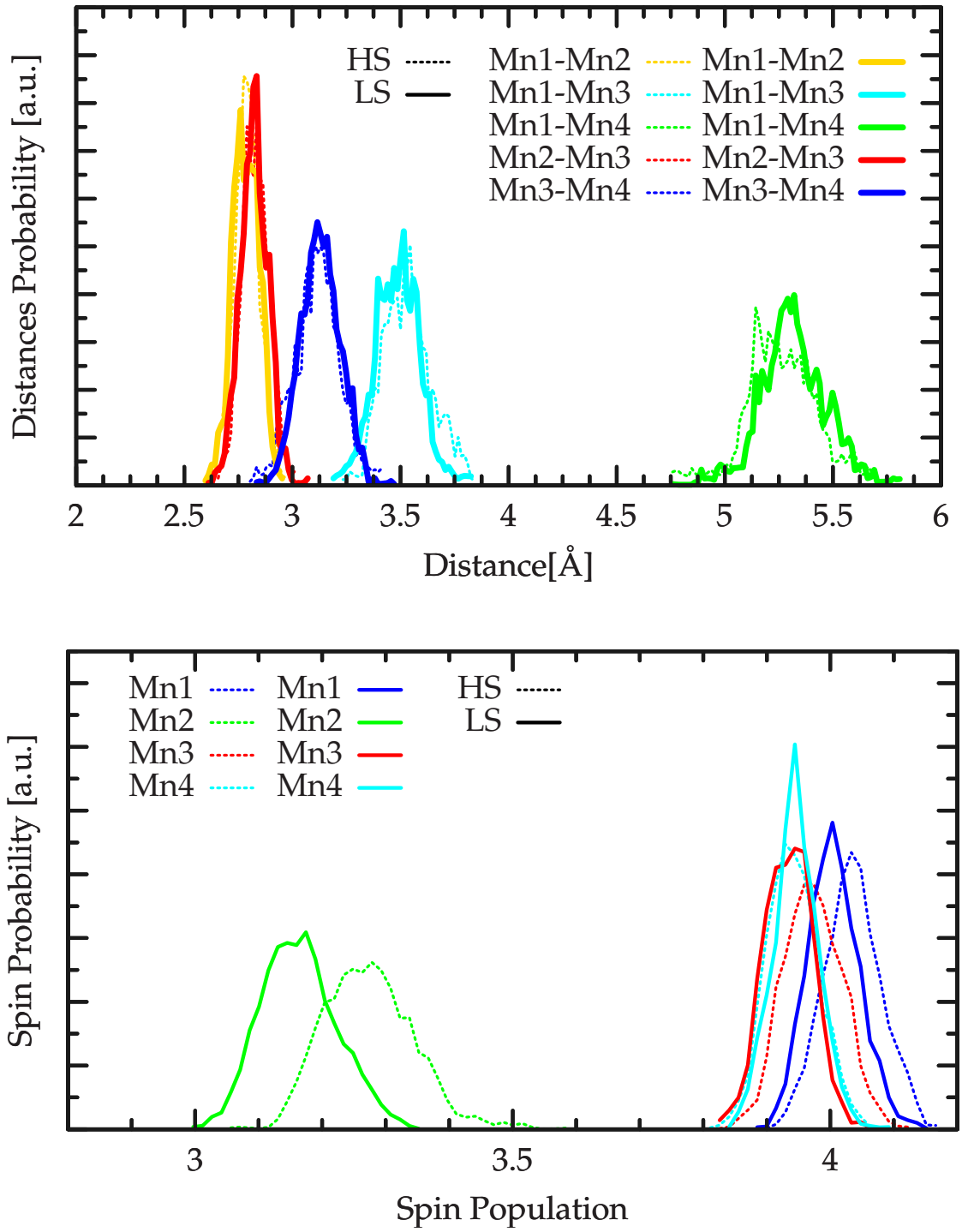

Fig.S1: Distance and spin distributions along QM/MM MD simulations. In the top panel the distribution of the Mn-Mn distances sampled in the QM/MM MD simulations of the S_4 state after O_2 release are shown for both HS and LS configurations. In the bottom panel the spin distribution of the four Mn ions sampled along the two HS and LS simulations are also reported.

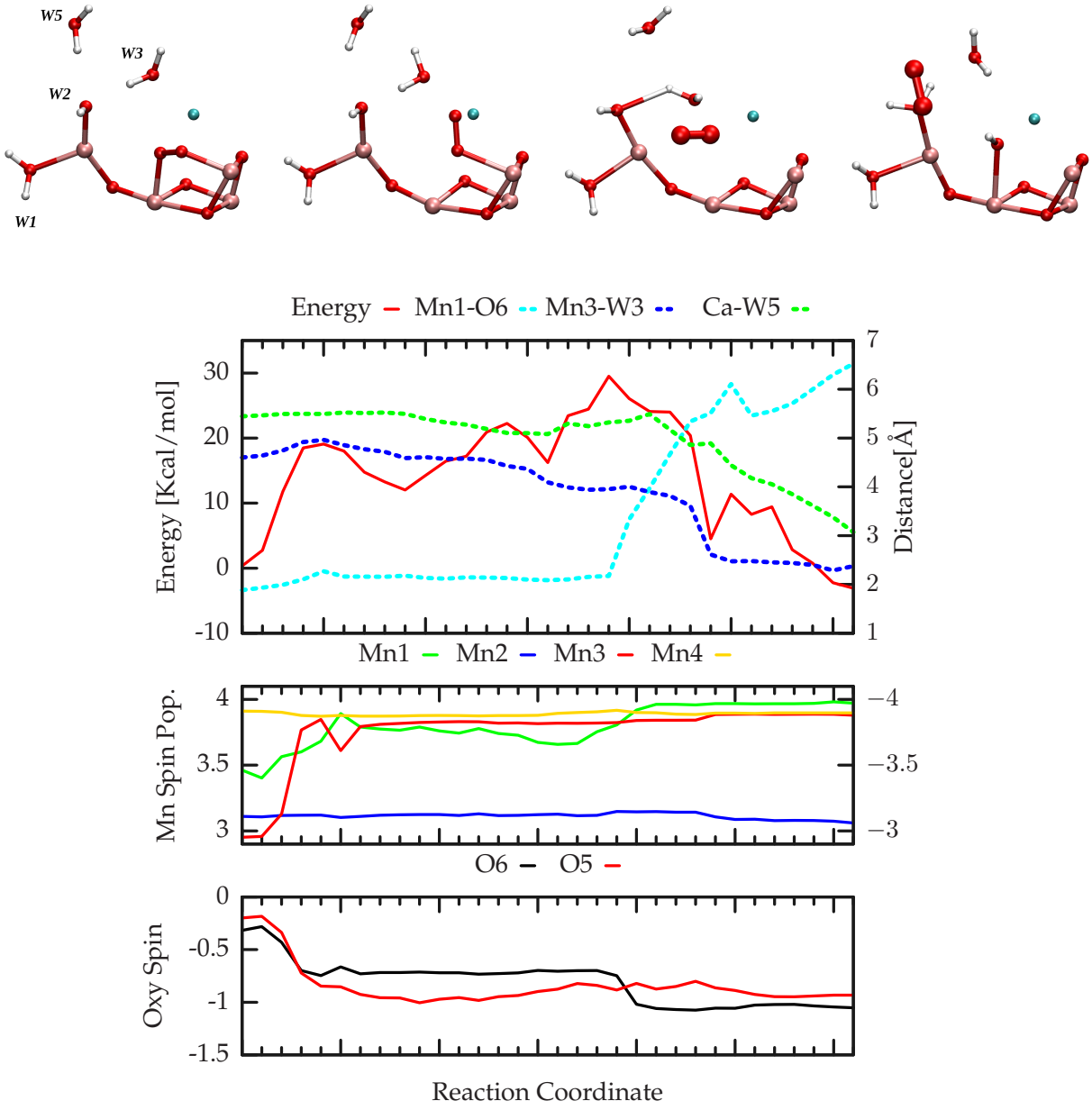

Fig.S2: Energy profile for the O_2 release coupled with W3 insertion. In the top panel representative structures of the reaction coordinate are shown. Below, the energy profile is reported for the LS configuration. Mn3-W3, Mn1-O6 and Ca-W5 distances are also shown as dashed lines. In the two bottom panels the spin populations of the four Mn ions and the two oxygen atoms O5 and O6 are also reported.

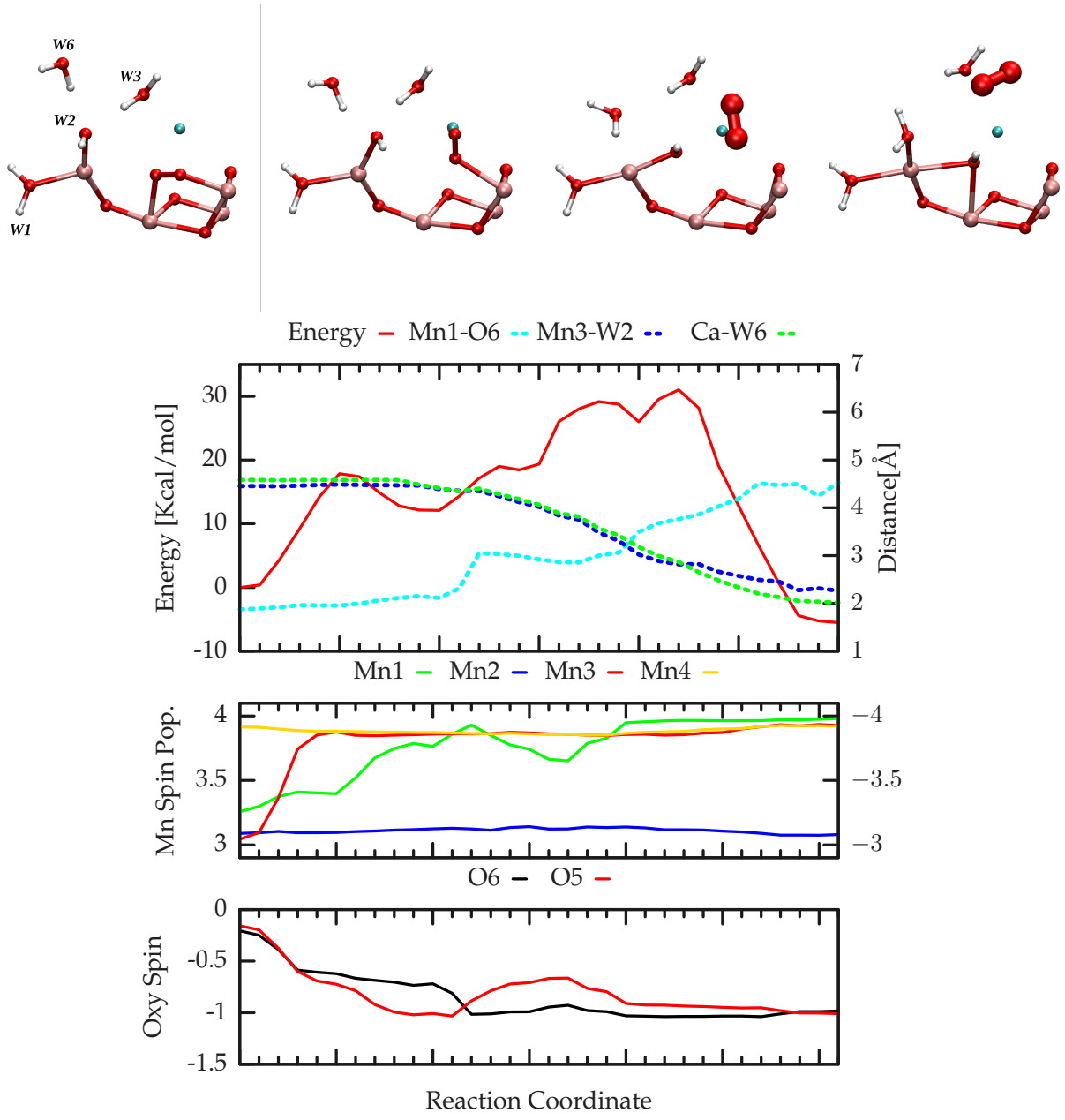

Fig.S3: Energy profile for the O_2 release coupled with W2 insertion. In the top panel representative structures of the reaction coordinate are shown. Below, the energy profile is reported for the LS configuration. Mn3-W2, Mn1-O6 and Ca-W6 distances are also shown as dashed lines. In the two bottom panels the spin populations of the four Mn ions and the two oxygen atoms O5 and O6 are reported.

References

(1) Laino, T.; Mohamed, F.; Laio, A.; Parrinello, M. *J. Chem. Theory Comput.* **2005**, *1*, 1176–1184.

(2) Hornak, V.; Abel, R.; Okur, A.; Strockbine, B.; Roitberg, A.; Simmerling, C. *Proteins* **2006**, *65*, 712–725.

(3) Wang, J.; Wolf, R. M.; Caldwell, J. W.; Kollman, P. A.; Case, D. A. *J. Comput. Chem.* **2004**, *25*, 1157–1174.

(4) Narzi, D.; Bovi, D.; Guidoni, L. *Proc. Natl. Acad. Sci. USA* **2014**, *111*, 8723–8728.

(5) Narzi, D.; Coccia, E.; Manzoli, M.; Guidoni, L. *Biophys. Chem.* **2017**, *229*, 93–98.

(6) Umena, Y.; Kawakami, K.; Shen, J.-R.; Kamiya, N. *Nature* **2011**, *473*, 55–60.

(7) Nosé, S. *J. Chem. Phys.* **1984**, *81*, 511–519.

(8) Nosé, S. *Mol. Phys.* **1984**, *52*, 255–268.

(9) Hoover, W. G. *Phys. Rev. A* **1985**, *31*, 1695–1697.

(10) Anisimov, V. I.; Zaanen, J.; Andersen, O. K. *Phys. Rev. B* **1991**, *44*, 943.

(11) Dudarev, S. L.; Manh, D. N.; Sutton, A. P. *Philos. Mag. B* **1997**, *75*, 613–628.

(12) Dudarev, S. L.; Botton, G. A.; Savrasov, S. Y.; Humphreys, C. J.; Sutton, A. P. *Phys. Rev. B* **1998**, *57*, 1505–1509.

(13) VandeVondele, J.; Hutter, J. *J. Chem. Phys.* **2007**, *127*, 114105.

(14) VandeVondele, J.; Krack, M.; Mohamed, F.; Parrinello, M.; Chassaing, T.; Hutter, J. *Comput. Phys. Comm.* **2005**, *167*, 103–128.

(15) Krewald, V.; Retegan, M.; Cox, N.; Messinger, J.; Lubitz, W.; DeBeer, S.; Neese, F.; Pantazis, D. A. *Chem. Sci.* **2015**, *6*, 1676–1695.

(16) Capone, M.; Bovi, D.; Narzi, D.; Guidoni, L. *Biochemistry* **2015**, *54*, 6439–6442.

(17) Capone, M.; Narzi, D.; Bovi, D.; Guidoni, L. *J. Phys. Chem. Lett.* **2016**, *7*, 592–596.

(18) Narzi, D.; Capone, M.; Bovi, D.; Guidoni, L. *Chem. Eur. J.* **2018**, *24*, 10820–10828.